FULL PAPER

Light Extraction of Organic Light Emitting Diodes by Defective Hexagonal-Close-Packed Array

*Won Hoe Koo, Wooram Youn, Peifen Zhu, Xiao-Hang Li, Nelson Tansu, and Franky So**

Defective silica sphere arrays having locally hexagonal-closed-packed structure but lack of long range ordering were incorporated into organic light emitting diodes as grating to extract the waveguided light trapped in the indium tin oxide/organic layers and the glass substrate. Using these defective hexagonal-closed-packed gratings for light extraction, broad band lambertian emitters are obtained due to the periodicity broadening and the random orientation in the gratings, resulting in enhancements in current and power efficiencies by a factor of 1.7 and 1.9, respectively.

1. Introduction

Light extraction in organic light emitting diodes (OLEDs) has been an active area of research because of significant power loss due to light waveguiding in the indium tin oxide (ITO)/organic layers (ITO/organic mode) and the glass substrate (substrate mode). While the substrate mode can easily be outcoupled by attaching a commercial microlens array or a light extraction film on the back of the substrate, extraction of the ITO/organic mode is much more challenging to achieve without deteriorating the device performance because it requires a modification of the internal structure inside the device such as low-index grids outside the transparent electrodes,[1] internal scattering structure of the organic layer,[2] preferred orientation of the transition dipole moments of the emitter film,[3] and Bragg diffraction gratings.[4–10] Bragg diffraction grating requiring incorporation of corrugated structure into OLEDs have been widely studied as one of most promising approaches, but it still has many issues to be solved for practical applications. For most photonic and grating structures used for light extraction, the outcoupled light is strongly directional depending on the specific emission wavelength, polar angle, and azimuthal angle because of their perfectly periodic microstructure.[4–10] In addition, fabrication of these corrugated structures requires ebeam lithography which is not compatible with low cost manufacturing. Recently, Koo et al. reported that a spontaneously formed buckling structure with a non-directional emission profile might provide a new approach to randomize with the directionality in photonic crystal structures.[11–14] In this paper, we demonstrate a light extraction scheme with an emission profile close to a Lambertian emitter by introducing defects into a hexagonal-close-packed (HCP) silica sphere arrays and thereby randomizing the directionality and broadening the periodicity. The defective silica sphere array having locally HCP structure but lack of long ordering was fabricated by simple low cost rapid convective deposition. Although Hyun et al. reported two dimensional (2D) titanium oxide (TiO_2) photonic crystal by the simple convective deposition for light extraction in polymer light emitting diodes, they did not address the effects of the defects involved in their periodic structure on light extraction, their 2D TiO_2 photonic crystal with flat surface was unable to outcouple the surface plasmon mode propagating at the interface between the organic and cathode layers.[15] Here, we demonstrate the effects of the defective HCP array on light extraction experimentally and theoretically, and finally report 70% and 90% enhancements in current and power efficiencies, respectively, without introducing particular spectral change over emission angles.

Dr. W. H. Koo, W. Youn, Prof. F. So
Department of Materials Science and Engineering
University of Florida
Gainesville, Florida, 32611-6400, USA
E-mail: fso@mse.ufl.edu
P. Zhu, X. H. Li, Prof. N. Tansu
Center for Optical Technologies
Department of Electrical and Computer Engineering
Lehigh University
Bethlehem, Pennsylvania, 18015, USA

DOI: 10.1002/adfm.201200876

2. Results and Discussion

2.1. Fabrication and Characterization of Defective HCP Structure

The HCP silica sphere array was prepared by the rapid convective deposition process which is applicable for low-cost and large scale production without using lithography.[16–19] 14% silica and 4% polystyrene binary suspension prepared by dispersing the 1.0- and 0.5-μm-diameter silica microspheres and 100-nm-diameter polystyrene nanospheres into distilled water were deposited with the deposition blade on glass substrates. **Figure 1**(a) shows the 0.5-μm-diameter silica sphere with the 100-nm-diameter polystyrene after deposition. After heat treatment of the sample at 140 °C for 4 minutes, the polystyrene spheres were melted to form a thin film embedded with a monolayer of silica spheres, thereby forming corrugated structures with periodicities corresponding to the size of the silica spheres, as seen in Figure 1(b) and (c). The depth of the corrugated structure was tuned by controlling the heat treatment time to reduce the polystyrene layer thickness, similar to the

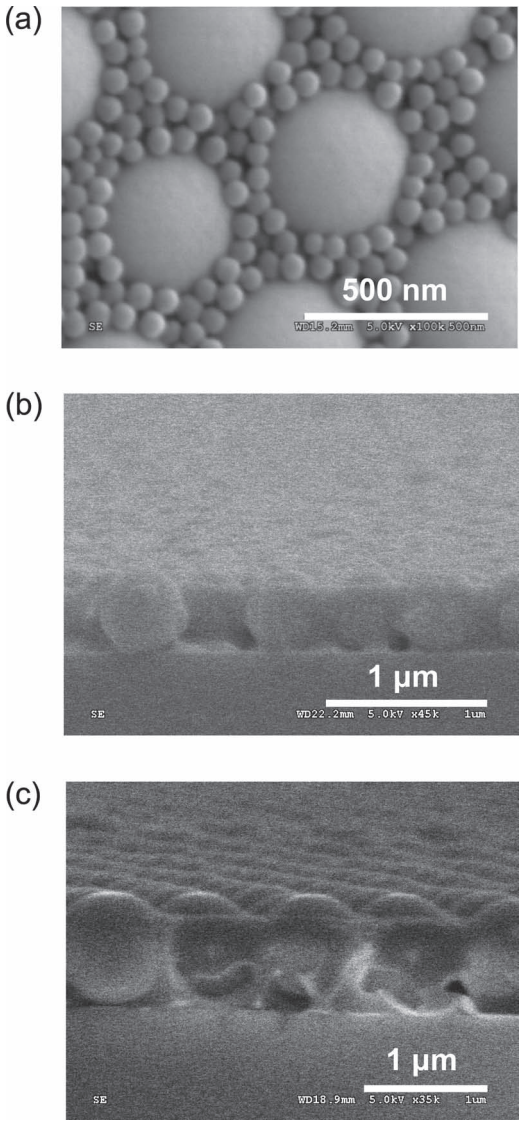

Figure 1. (a) Scanning electron microscopy (SEM) image on the 0.5-μm-diameter silica sphere mixed with the 100 nm polystyrene sphere before heat treatment. (b) and (c) Cross-sectional view of SEM images on the 0.5- and 1.0-μm-diameter silica array template after heat treatment at 140 °C for 4 minutes, respectively.

process described in Reference 19. While the diffraction efficiency of grating generally increases with the depth of grating, we selected the depth of ~185 nm and ~75 nm for the 1.0- and 0.5-μm gratings because too high depth of grating causes a device failure due to high leakage current paths. To form a corrugated structure for OLED fabrication, a polydimethylsiloxane (PDMS) replica was first made using the silica sphere array substrate as a template. Subsequently, the PDMS replica was stamped onto a UV-curable resin coated glass substrate. Finally, the corrugated resin layer having locally HCP structure but lack of long ordering and a flat resin layer on the 0.1-mm-thick glass substrates were used for grating and reference devices, respectively.

Figure 2(a) and (b) show the atomic force microscopy (AFM) images of the 1.0- and 0.5-μm-diameter silica sphere array templates respectively along with the fast Fourier transform (FFT) patterns as inserts. Although the local HCP areas retain the hexagonal FFT patterns, defects in the array break the long range hexagonal symmetry and generate a ring pattern over the entire area. The FFT patterns indicate that the defective HCP array pattern forms the grating vectors in all azimuthal angles, allowing diffractions of waveguided light in all azimuthal angles.[11–14] The line profiles in the AFM images show that the local HCP areas in the corrugated templates have the periodicities of 1.0 and 0.5 μm corresponding to the diameters of the silica spheres. However, the power spectral density from the whole area in Figure 2(c) indicate that the 1.0 and 0.5 μm templates actually have peak periodicities of 0.46 ± 0.04 and 0.9 ± 0.1 μm. The depths of the corrugated templates were 180 ~ 190 and 70 ~ 80 nm for the 1.0 and 0.5 μm templates, respectively, but the depths of the corrugated resin layers imprinted from the template were reduced slightly to 170 ~ 180 and 60 ~ 70 nm respectively, while their periodicities of 0.46 ± 0.04 and 0.9 ± 0.1 μm were maintained. The calculated surface area ratios, expressing the increment of the corrugated surface area relative to the flat surface area, were ~12% and ~8% for the 1.0 and 0.5 μm corrugated resin layers.

2.2. OLED Devices with 1.0 μm Grating

To fabricate the OLEDs, the following layers were deposited on the corrugated and flat resin layers coated glass substrates: a 120-nm-thick ITO, a 50-nm-thick NPB (N,N'-bis(naphthalene-1-yl)-N,N'-bis-(phenyl)benzidine)), a 60-nm-thick Alq_3 (tris-(8-hydroxyquinoline)-aluminum), a 1.0-nm-thick lithium fluoride (LiF), and a 100-nm-thick aluminum (Al). **Figure 3**(a) shows the device structure and Figure 3(b) shows the distributions of the electric field intensities for one transverse-electric (TE_0) and two transverse-magnetic (TM_0 and TM_1) waveguide modes, which were calculated by the tranfer matrix method.[11] Generally, the diffraction efficiency of a grating is proportional to the electric field intensity in the grating region.[20] Because the corrugated structure is maintained over all layers from the resin to the Al layer, effective outcoupling of the thin film guided modes is expected.

The typical current densities (mA/cm^2) and luminances (cd/m^2) for the devices with and without 1.0 μm grating are plotted as a function of applied voltage in **Figure 4**(a). The 1.0 μm grating device shows a higher current density and a higher luminance at a constant voltage compared with the reference device. The leakage current of the grating device below turn-on voltage showed little difference with that of the reference device on a log-log scale, indicating smooth surface of the corrugated structure in the grating device. (Supporting information) Because the surface area of the grating devcie is increased slightly by ~12%, the much higher enhancemnt of the current density in the grating device cannot be explained by considering only the surface area enhancement. In general, it is reported that a corrugated OLED have a higher current density because of the enhanced electric

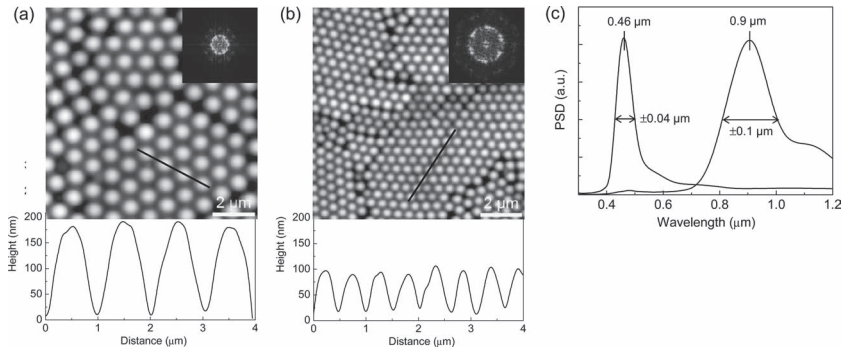

Figure 2. AFM images and line profiles on the (a) 1.0- and (b) 0.5-μm-diameter silica sphere arrays template (Dimensions, 10 × 10 μm). Inset: The FFT pattern of each image. The solid line in the image corresponds to the line profile below the image. (c) Power spectral density from FFTs as a function of wavelength for 1.0 and 0.5 μm templates.

field due to non-uniformity of the organic layer thicknesses in a corrugated structure.[9,11,21] Despite of the increased current density, the higher enhancment of the luminace in the grating device represents the extraction of the waveguide modes. The current (cd/A) and power efficiencies (lm/W) at a current density of 40 mA/cm^2 are 2.6 cd/A and 1.64 lm/W for the reference device and 3.5 cd/A and 2.5 lm/W for the grating device (Figure 4(b)). The grating device shows 35% and 50% enhancements in the current and power efficiencies compared to the reference devices. The higher enhancement in the power efficiency than the current efficiency is due to the lower operating voltage in the grating devices, as shown in Figure 4(a). The electroluminescence (EL) spectra of the grating and reference devices at normal direction show that there is no spectral change due to the 1.0-μm grating (inset of Figure 4(c)). Dividing the EL intensity of the grating device by that of the reference device, the enhancement ratio for the emission wavelengths is obtained and the results are shown in Figure 4(c). The enhancement ratio is fairly uniform across the EL spectrum with slightly higher intensities at around 500 and 650 ~ 700 nm.

In order to elucidate the dependence of the enhancement ratio on the emission wavelength, we calculated the dispersion curves of the TE_0, TM_0 and TM_1 modes and the results are shown in Figure 4(d). The dispersion curve with the light lines for air and glass substrate can be divided into three regions: *air*, *substrate*, and *ITO/organic* modes. According to the Bragg grating equation, the large in-plane wave vectors of the TE_0, TM_0 and TM_1 modes can be reduced by the grating vector which is inversely proportional to the periodicity of grating.[11–14] The length of the small arrows in Figure 4(d) represents the magnitude of the grating vectors by the periodicity of 0.9 and 0.8 μm from the periodicity range of 0.9 ± 0.1 μm. While the small grating vector due to the large periodicity is only able to transfer the *ITO/organic* mode to the *substrate* mode by the first order diffraction, a fraction of the enhanced *substrate* mode can be outcoupled to the *air* mode by multiple scattering with the corrugated Al layer on a thin glass substrate (0.1 mm).[13] We believe that the efficiency enhancement by the 1.0 μm grating is mainly caused by the extraction of the *substrate* mode by scattering, which gives rise to the broad enhancement of the EL intensity over all emission wavelengths in Figure 4(c). The slightly higher intensities at around 500 and 650 ~ 700 nm in Figure 4(c) are related to the transfer of the TM_1 mode to the *substrate* mode upto below ~520 nm along with the TE_0 and the second-order diffraction of TE_0 by the grating vectors from $k_{0.8\mu m}$ to $k_{0.9\mu m}$ above 630 nm, respectively. Since the TM_0 mode as the surface plasmon mode has the characteristics of the strong absorption, the large periodicity of 0.9 ± 0.1 μm can not extract the TM_0 mode effectively.[12]

2.3. OLED Devices with 0.5 μm Grating

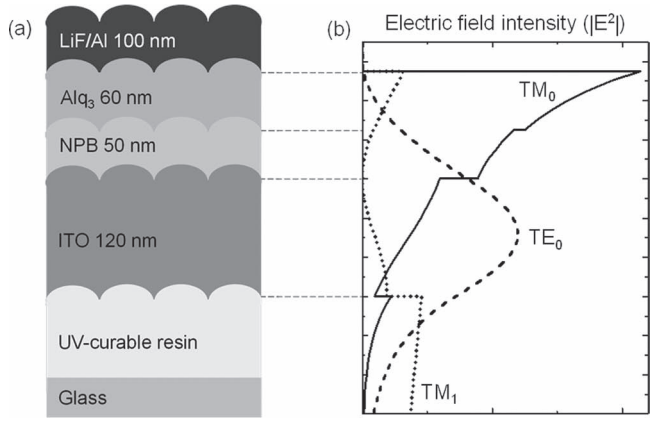

Figure 3. (a) Currgated device structure and (b) distributions of electric field intensity across the layers for TE_0 (- -), TM_0 (—), and TM_1 (····) waveguide modes in a flat structure, calculated by transfer matrix method.

With the 0.5 μm grating, the TE_0, TM_0 and TM_1 modes can be more effectively outcoupled because of the larger grating vector to counter their large in-plane wave vectors. **Figure 5**(a) shows the current densities and luminances for the 0.5 μm grating device and the reference device. Similar to the 1.0 μm grating device, the 0.5 μm grating device exhibits a higher current density and higher luminance than those of the reference device. However, the enhancement of the current density in the 0.5 μm grating device is lower than that in the 1.0 μm grating device because of the lower surface area ratio of the 0.5 μm grating (~8%) than the 1.0 μm grating (~12%). The current and power efficiencies at a current density of 40 mA/cm^2 in Figure 5(b) are 2.57 cd/A and 1.58 lm/W for the reference devices, and 4.38 cd/A and 2.95 lm/W for the grating devices, respectively. Enhancements of ~70% and ~90% were achieved for the current and power efficiencies due to the 0.5 μm grating. The larger enhancement of the 0.5 μm grating device, compared to the 1.0 μm grating device, is associated with the larger grating vector of the 0.5 μm grating. The EL

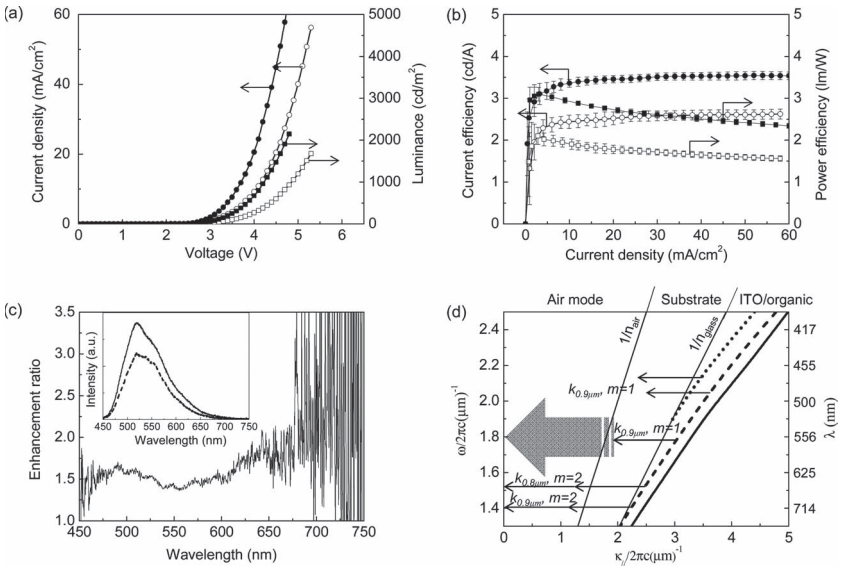

Figure 4. (a) Current density (mA/cm^2) and luminance (cd/m^2) and (b) Current efficiency (cd/A) and power efficiency (lm/W) for the 1.0 μm grating (filled symbols) and reference (open symbols) devices. (c) Enhancement ratio of EL intensity, plotted by dividing the spectrum of the grating device by that of the reference devices. Inset: EL spectra of the grating (—) and reference (- -) devices. (d) Dispersion curves of the TE_0 (- -), TM_0 (—), and TM_1 (····) modes by transfer matrix method. It was assumed that the refractive index of a resin layer ($n = 1.56$) is equal to that of a glass substrate ($n = 1.52$). The thin solid lines represent the light lines for air and glass substrate. The small arrows indicate the grating vectors $k_{0.9\mu m}$ and $k_{0.8\mu m}$ from the periodicity distribution of 0.9 ± 0.1 μm in the 1.0 μm grating, and *m = 1, 2* means the first- and second-order diffraction. A large arrow describes the extraction of the *substrate* mode, irrespective of the length of the arrow.

2.4. Angular Dependence of Emitting Light with and Without Hemisphere Lens

The EL spectra of the reference and 0.5 μm grating devices for 0°, 20°, 40°, and 60° are shown in **Figure 6**(a). All EL intensities of the 0.5 μm grating devices are enhanced over all emission wavelengths irrespective of the emission angles because the ITO/organic modes and the substrate mode are extracted by the 0.5 μm grating with the broad periodicity and the random orientation. In order to more effectively extract the substrate mode, a hemisphere lens was used. By integrating the EL spectrum, the angular dependences of emitting light for the reference, 1.0, and 0.5 μm grating devices with (filled circle) and without (open circle) the hemisphere lens are shown in Figure 6(b), (c), and (d), respectively. The emitting light intensities of each device for all emission angles were normalized by the intensity of each device without the hemisphere lens at normal direction. Both the reference and 1.0 μm grating devices without the hemisphere exhibit nearly Lambertian emission pattern. Since the grating vector by the 1.0 μm grating is too small to directly extract the ITO/organic mode by the first-order diffraction, the indirect extraction of the enhanced substrate mode via the multiple

spectra of the grating and reference devices at normal direction again show a broad enhancement over all emission wavelengths (inset of Figure 5(c)). The enhancement ratio in Figure 5(c) represents two strong intensities at around 470 and 700 nm. It should be noted that the enhancements at both ends of the spectrum are slightly larger compared to the 1.0 grating device. According to the dispersion curve in Figure 5(d), the 0.5 μm grating having the periodicity range of 0.46 ± 0.04 μm can extract the TE_0 and TM_0 modes into the normal direction through the second-order diffraction by the grating vectors from $k_{0.46\mu m}$ to $k_{0.5\mu m}$ at around 470 nm and the first-order diffraction by the grating vectors from $k_{0.42\mu m}$ to $k_{0.46\mu m}$ at around 700 nm, while those modes at all emission wavelengths can be outcoupled to various angles through the first- and second-order diffractions by the wide range of the grating vectors. The *substrate* mode also can be outcoupled through the multiple scattering between the corrugated Al cathode layer and the thin glass substrate, contributing to the overall enhancement for all emission wavelengths, as seen in Figure 5(c).

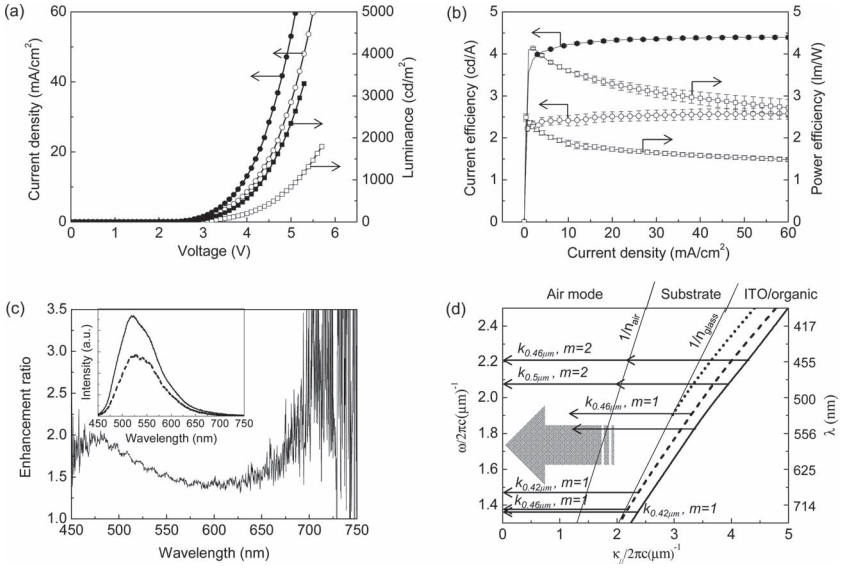

Figure 5. (a) Current density (mA/cm^2) and luminance (cd/m^2) and (b) Current efficiency (cd/A) and power efficiency (lm/W) for the 0.5 μm grating (filled symbols) and reference (open symbols) devices. (c) Enhancement ratio of EL intensity. Inset: EL spectra of the grating (—) and reference (- -) devices. (d) Dispersion curves of the TE_0 (- -), TM_0 (—), and TM_1 (····) modes. The small arrows indicate the grating vectors $k_{0.42\mu m}$, $k_{0.46\mu m}$, and $k_{0.5\mu m}$ from the periodicity distribution of 0.46 ± 0.4 μm in the 0.5 μm grating, and *m = 1, 2* means the first- and second-order diffraction. A large arrow describes the extraction of the *substrate* mode, irrespective of the length of the arrow.

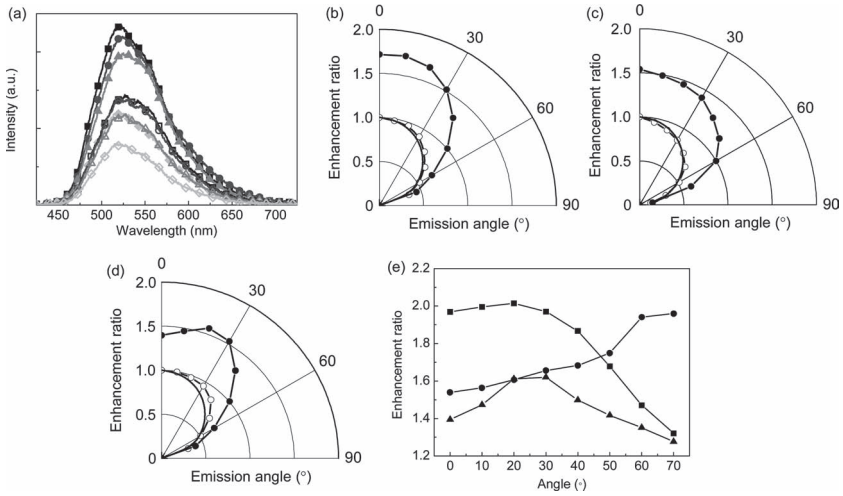

Figure 6. (a) EL spectra of the reference (open symbols) and the 0.5 μm (filled symbols) grating without a hemisphere lens for the emission angles of 0° (square), 20° (circle), 40° (triangle), and 60°(diamond). Angular dependence of emitting light for (b) the reference, (c) 1.0 μm, (d) 0.5 μm grating devices with (filled circle) and without (open circle) the hemisphere lens. The solid line represents a Lambertian emission pattern. The emitting light intensities of each device with and without lens for all emission angles were normalized by the intensity of each device without lens at normal direction. (e) Enhancement ratio of the EL intensity by the hemisphere lens for the reference (square), 1.0 μm (circle), and 0.5 μm (triangle) grating devices, by dividing the EL intensity of the device with the hemisphere lens by that of the device without the hemisphere lens in (b)~(d).

scattering gives rised to the non-characteristic emission profile in Figure 6(c). However, the 0.5 μm grating device shows the broader distribution, compared with the Lambertian emission pattern, particularly at around 40° which corresponds the first-order diffraction angle of the TE_0 and TM_0 modes around the main emission peak of 530 nm by the grating periodicicty of 0.46 μm. It should be noted that while OLEDs fabricated on a conventional grating or photonic crystal structure with a short and long range order hexagonal symmetry give distinct butterfly wing emission patterns,[22,23] the emission profiles of our OLEDs fabricated on defective HCP array patterns do not show a particular polar- and azimuthal angle dependence because of the broadening of the periodicity and the random orientation from the defective array pattern.

With the hemisphere lens, the 1.0 and 0.5 μm grating devices in Figure 6(c) and (d) represent different characteristic emission profiles from the reference device in Figure 6(b). These indicate that the grating on the thin glass redistributes the substrate mode by transferring the ITO/organic mode to the substrate mode and extracting the substrate mode, depending on its periodicity. In order to understand the mode distribution, we define the enhancement ratio by dividing the EL intensity of the device with the hemisphere lens by that of the device without the hemisphere lens. Figure 6(e) shows the enhancement ratios for the reference (square), 1.0 μm (circle) and 0.5 μm (triangle) grating devices. Please, note that the smaller enhancement of the grating devices than the reference device in Figure 6(e) is caused by the higher efficiency of the grating devices without the hemisphere lens than the reference device without the hemisphere lens. While the enhancement ratio of the reference device with the hemisphere lens generally decreases with increasing emission angles, that of the 1.0 μm grating device with the hemisphere lens increases rather than decreases, possibly because the first-order diffraction by the 1.0 μm grating can only transfer the *ITO/organic* mode to the *substrate* mode. The enhancement ratio of the 0.5 μm grating device with the hemisphere lens increases up to 20 ~ 30° and then decreases as the emission angle increases further, reflecting the extraction of the *ITO/organic* mode by the 0.5 μm grating, contrary to the 1.0 μm grating.

The reference device with the hemisphere lens shows the enhancement of 77% in the integrated intensity over all emission angles, compared to that without the hemisphere lens, while the 1.0 and 0.5 μm grating devices with the hemisphere lens show the enhancements of 67% and 48%, compared to each device without the hemisphere lens, indicating that a fraction of the *ITO/organic* modes in the grating devices are indeed extracted to the air mode. Finally, the power efficiencies of the 1.0 and 0.5 μm grating devices with lens were enhanced by a factor of ~2.5 ($= 1_{\text{reference}} \times 1.6_{\text{power efficiency}} \times 1.67_{\text{lens}}$) and ~2.8 ($= 1_{\text{reference}} \times 1.9_{\text{power efficiency}} \times 1.48_{\text{lens}}$), respectively, compared with the reference device without the hemisphere lens.

3. Conclusions

In summary, a defective silica sphere array pattern having locally HCP structure but lack of long ordering was fabricated by rapid convective deposition. The defective silica array pattern was incorporated into the devices as grating to extract the ITO/organic modes and additionally the substrate mode via a thin glass substrate. Despite of the insufficient grating vector, the 1.0 μm grating devices showed the 35% and 50% enhancements in the current and power efficiencies by transferring the ITO/organic modes to the substrate mode and then scattering the substrate mode. The 0.5 μm grating devices with the stronger grating vector were able to effectively outcouple the ITO/organic modes by the first- and second-order diffractions with the scattered substrate mode, thereby improving the current and power efficiency by 70% and 90%, respectively, without spectral changes and directionality. With the low-cost and large-area processing, the defective HCP silica array pattern can supply a practical solution for light extraction in the field of OLED applications.

4. Experimental Section

Defective HCP grating fabrication: Silica sphere array templates were fabricated by depositing a suspension consisting of either 1.0- or 0.5-μm-diameter silica spheres and 100-nm-diameter polystyrene spheres on glass substrate by rapid convective deposition. The details of the silica/polystyrene sphere array deposition are described in detail

in references.[16–19] In these experiments, we employed 14% silica and 4% polystyrene binary suspension prepared by dispersing the 1.0- and 0.5-μm diameter silica microspheres and 100-nm diameter polystyrene nanospheres into distilled water. Then, the suspension was immersed in the ultrasonic bath for 1 hour and thoroughly shaken by the vortex for 1 min. Prior to deposition, the glass substrate was cleaned by using piranha solution (volume ratio of 5:1 for sulfuric acid/hydrogen peroxide) and distilled water. The back and bottom edges of glass deposition blade were treated for ensuring hydrophobic surfaces by adding a thin coating with parafilm in order to control the wetting region of the meniscus droplet. During the deposition, a 7.0-μL droplet silica/polystyrene binary suspension was firstly injected between the substrate and the blade forming a wedge with the substrate at the angle 55°. Afterwards, the blade swept across substrate at a speed of 62.5 μm/s by a linear motor. After deposition, the sample was heated at 140 °C to melt the polystyrene spheres, which would fill up the gap between the silica microspheres to form the planar polystyrene layer. By using this process, we fabricated silica/polystyrene arrays templates with silica sphere diameters of 1.0- and 0.5 μm employing polystyrene thicknesses of 815 nm and 425 nm, respectively. These 1.0 and 0.5 μm silica sphere array substrates were used as a template on which PDMS was poured and cured at 60 °C for 2 hours to form the PDMS replica. To fabricate the resin coated substrate for OLED fabrication, a UV-curable resin layer (Norland Optical Adhesive 81) was spincoated on the 0.1-mm-thick glass substrates and subsequently cured by UV irradiation for 5 minutes, a drop of resin was placed on the resin-coated substrates. Then the silica sphere array patterns of the PDMS replicas were transferred to UV-curable resin layers by imprinting technique. Finally, the corrugated resin layer and a flat resin layer coated glass substrates were used for grating and reference devices, respectively.

Device fabrication and measurement: For device fabrication, the following layers were deposited on the corrugated and flat resin layers: a 120-nm-thick ITO, a 50-nm-thick NPB (N,N′-bis(naphthalene-1-yl)-N,N′-bis-(phenyl)benzidine)), a 60-nm-thick Alq_3 (tris-(8-hydroxyquinoline)-aluminum), a 1.0-nm-thick lithium fluoride (LiF), and a 100-nm-thick aluminum (Al). The devices with the emitting area of 2 mm × 2 mm were encapsulated with glass and UV-curable sealant in a glove box under N_2 atmosphere. In order to extract the *substrate* mode, a hemisphere lens with a diameter of 3 mm was attached on the back of the glass substrate.

Electroluminescence (EL) spectra were recorded with a source meter (Keithley 2400) and a spectrometer (Ocean Optics HR4000). The angular emission patterns were measured by integrating the EL spectra of devices according to emission angles. A perfect hemisphere lens with a diameter of 5 mm and a refractive index of 1.52 was attached on glass substrate of devices by an index matching gel.

Supporting Information

Supporting Information is available from the Wiley Online Library or from the author.

Acknowledgements

The authors would like to acknowledge the support of Department of Energy Solid State Lighting Program (Contract number: DE-FG0207ER46464).
The authors would like to acknowledge the support of the Department of Energy Office of Energy Efficiency and Renewable Energy (Contract Number: DE-EE0001522). The authors would also like to acknowledge Dr. Renbo Song and Mr. Le Zhao of Department of Electrical and Computer Engineering at Lehigh University for their assistance in preparing part of the microlens arrays template, and Prof. James F. Gilchrist and Dr. Pisist Kumnorkaew of Department of Chemical Engineering at Lehigh University for technical assistance in colloidal suspension preparation.

Received: March 28, 2012
Published online: May 10, 2012

[1] Y. Sun, S. R. Forrest, *Nat. Photonics* **2008**, *2*, 483.
[2] T. W. Lee, O. O. Park, Y. C. Kim, *Org. Electron.* **2007**, *8*, 317.
[3] J. Frischeisen, D. Yokoyama, C. Adachi, W. Brütting, *Appl. Phys. Lett.* **2010**, *96*, 073302.
[4] M. Fujita, K. Ishihara, T. Ueno, T. Asano, S. Noda, H. Ohata, T. Tsuji, H. Nakada, N. Shimoji, *Jpn. J. Appl. Phys., Part 1.* **2005**, *44*, 3669.
[5] J. M. Ziebarth, A. K. Saafir, S. Fan, M. D. Mcgehee, *Adv. Func. Mater.* **2004**, *14*, 451.
[6] B. J. Matterson, J. M. Lupton, A. E. Safonov, M. G. Salt, W. L. Barnes, I. D. Samuel, *Adv. Mater.* **2001**, *13*, 123.
[7] P. A. Hobson, J. A. E. Wasey, I. Sage, W. L. Barnes, *IEEE J. Sel. Top. Quantum Electron.* **2002**, *8*, 378.
[8] S. M. Jeong, F. Araoka, Y. Machida, Y. Takanishi, K. Ishikawa, H. Takezoe, S. Nishimura, G. Suzaki, *Appl. Phys. Lett.* **2008**, *92*, 083307.
[9] S. M. Jeong, F. Araoka, Y. Machida, Y. Takanishi, K. Ishikawa, H. Takezoe, S. Nishimura, G. Suzaki, *Jpn. J. Appl. Phys.* **2008**, *47*, 4566.
[10] K. Ishihara, M. Fujita, I. Matsubara, T. Asano, S. Noda, H. Ohata, A. Hirasawa, H. Nakada, N. Shimoji, *Appl. Phys. Lett.* **2007**, *90*, 111114.
[11] W. H. Koo, S. M. Jeong, F. Araoka, K. Ishikawa, S. Nishimura, T. Toyooka, H. Takezoe, *Nat. Photonics* **2010**, *4*, 222.
[12] W. H. Koo, S. M. Jeong, S. Nishimura, F. Araoka, K. Ishikawa, T. Toyooka, H. Takezoe, *Adv. Mater.* **2011**, *23*, 1003.
[13] W. H. Koo, F. Araoka, K. Ishikawa, S. M. Jeong, S. Nishimura, T. Toyooka, H. Takezoe, *Appl. Phys. Express* **2011**, *4*, 032101.
[14] W. H. Koo, S. Y. Boo, S. M. Jeong, S. Nishimura, F. Araoka, K. Ishikawa, T. Toyooka, H. Takezoe, *Org. Electron.* **2011**, *12*, 1177.
[15] W. J. Hyun, H. K. Lee, S. S. Oh, O. Hess, C. G. Choi, S. H. Im, O. O. Park, *Adv. Mater.* **2011**, *23*, 1846.
[16] Y. K. Ee, P. Kumnorkaew, R. A. Arif, H. Zhao, J. F. Gilchrist, N. Tansu, *Appl. Phys. Lett.* **2007**, *91*, 221107–1.
[17] P. Kumnorkaew, Y. K. Ee, N. Tansu, J. F. Gilchrist, *Langmuir* **2008**, *24*, 12150.
[18] Y. K. Ee, P. Kumnorkaew, R. A. Arif, J. F. Gilchrist, N. Tansu, *IEEE J. Sel. Topics Quantum Electron.* **2009**, *15*, 221107–1.
[19] X. H. Li, R. B. Song, Y. K. Ee, P. Kumnorkaew, J. F. Gilchrist, N. Tansu, *IEEE Photonics Journal* **2011**, *3*, 489.
[20] J. M. Ziebarth, M. D. McGehee, *J. Appl. Phys.* **2005**, *97*, 064502.
[21] M. Fujita, T. Ueno, K. Ishihara, T. Asano, S. Noda, H. Ohata, T. Tsuji, H. Nakada, N. Shimoji, *Appl. Phys. Lett.* **2004**, *85*, 5769.
[22] S. Jeon, J. W. Kang, H. D. Park, J. J. Kim, J. R. Youn, J. Shim, J. H. Jeong, D. G. Choi, K. D. Kim, A. O. Altun, S. H. Kim, Y. H. Lee, *Appl. Phys. Lett.* **2008**, *92*, 223307.
[23] A. O. Altun, S. Jeon, J. Shim, J. H. Jeong, D. G. Choi, K. D. Kim, J. H. Choi, S. W. Lee, E. S. Lee, H. D. Park, J. R. Youn, J. J. Kim, Y. H. Lee, J. W. Kang, *Org. Electron.* **2010**, *11*, 711.